Electromagnetic transition strengths in ^{156}Dy

O. Möller,[1] A. Dewald,[1] P. Petkov,[1,2] B. Saha,[1] A. Fitzler,[1] K. Jessen,[1] D. Tonev,[1,2] T. Klug,[1] S. Heinze,[1] J. Jolie,[1] P. von Brentano,[1] D. Bazzacco,[3] C. A. Ur,[3,*] E. Farnea,[3,4] M. Axiotis,[4] S. Lunardi,[3] G. de Angelis,[4] D. R. Napoli,[4] N. Marginean,[4] T. Martinez,[4] M. A. Caprio,[5] and R. F. Casten[5]

[1]*Institut für Kernphysik der Universität zu Köln, D-50937 Köln, Germany*

[2]*Bulgarian Academy of Sciences, Institute for Nuclear Research and Nuclear Energy, BG-1784 Sofia, Bulgaria*

[3]*Dipartimento di Fisica and INFN, Sezione di Padova, Padova, Italy*

[4]*INFN, Laboratori Nazionali di Legnaro, Legnaro, Italy*

[5]*Wright Nuclear Structure Laboratory, Yale University, New Haven, Connecticut, USA*

(Received 8 May 2006; published 22 August 2006)

Reliable and precise lifetimes of excited states in ^{156}Dy were measured by means of the recoil distance Doppler-shift technique in the coincidence mode. The experiment was performed at the Laboratori Nazionali di Legnaro with the GASP array and the Cologne coincidence plunger apparatus using the reaction ^{124}Sn(^{36}S,4n)^{156}Dy at a beam energy of 155 MeV. New values of the branching ratios of transitions depopulating the levels of the first excited band have been derived. The measured transition probabilities of ^{156}Dy in the ground-state band and the first excited band as well as the energy spectra are compared to the predictions of the recently proposed X(5) model and to an interacting boson approximation fit. The comparison reveals a different behavior of the intraband transition strengths and indicates a possible coexistence of a normal deformed ground-state band and an X(5)-like first excited band. It also reveals that in ^{156}Dy, the γ degree of freedom plays a more important role than it does in the well-established X(5) nuclei with $N = 90$. A fit of the data using the general collective model suggests that a deeper collective potential $V(\beta, \gamma)$ may also be a reason for the differences in the spectroscopic properties of ^{156}Dy and those nuclei.

DOI: 10.1103/PhysRevC.74.024313 PACS number(s): 21.10.Tg, 23.20.Lv, 27.70.+q

I. INTRODUCTION

The position of ^{156}Dy in a transitional region between spherical and deformed nuclei has attracted much experimental and theoretical interest over the last decades. A significant part of the corresponding studies was dedicated to the high-spin phenomena observed in this nucleus. In the present work, we concentrate on the ground-state band and the first excited band up to the moderate spin of about 16$\hbar$. These states were investigated already in the early seventies. In the works of Andrews *et al.* [1] and Lieder *et al.* [2], the interesting phenomenon of the crossing between the first excited band (or β band) and the S band was studied. The S band becomes yrast at the $I^\pi = 16^+$ level, where the levels of the continuation of the ground-state band (g.s.b.) start to form the yrare sequence. A portion of the level scheme of ^{156}Dy relevant to the present study is displayed in Fig. 1. The lifetimes of the yrast states up to high spins were measured by Ward *et al.* [4] and Emling *et al.* [5,6]. The results of these works implied rotationally induced shape changes affecting the parameters β and γ of the intrinsic quadrupole deformation. These changes were supposed to lead to irregularities of the collectivity, expressed through the $B(E2)$ values, in the spin region below $I^\pi = 16^+$. The purpose of the present work is to re-measure the lifetimes of the levels in the ground-state band and to determine for the first time lifetimes in the first excited band by using the recoil distance Doppler-shift method (RDDS) [7] and thus to verify the earlier suggested irregularities in the $B(E2)$ values. One of the reasons for doing this is that many theoretical calculations using mean-field approaches, e.g., Refs. [8–11], cannot reproduce such significant irregularities in the collectivity in the spin region considered (up to 14–16$\hbar$). Apart from this interesting physical topic, our work has been additionally stimulated by advances in experimental techniques which make possible the use of large multidetector arrays and provide the analysis with data of higher statistics. The development of the differential decay curve method (DDCM) ensures an adequate analysis tool for the data taken in coincidence mode [12,13].

Another important motivation for the present experimental work was the introduction of the new X(5) symmetry at the critical point of the SU(3)-U(5) phase transition [14]. This new symmetry had been experimentally established in ^{152}Sm [15] and ^{150}Nd [16] for the first time and was later also used to characterize the neighboring $N = 90$ nucleus ^{154}Gd [17]. The isotone ^{156}Dy was also regarded as a promising candidate for exhibiting the characteristic X(5) features. The present work aimed to supply further experimental data, especially electromagnetic transition probabilities, to allow stringent tests of the X(5) predictions for ^{156}Dy.

II. EXPERIMENT

To populate excited states in ^{156}Dy, the reaction ^{124}Sn(^{36}S,4n) at a beam energy of 155 MeV was used. The beam was provided by the XTU tandem of the Laboratori Nazionali di Legnaro, Italy. The target and stopper foils were mounted in the Cologne coincidence plunger [18] in which the change of the target-to-stopper distance is realized by moving the target holder. The constancy of the preset distance

*On leave from NIPNE Bucharest.

 ©2006 The American Physical Society

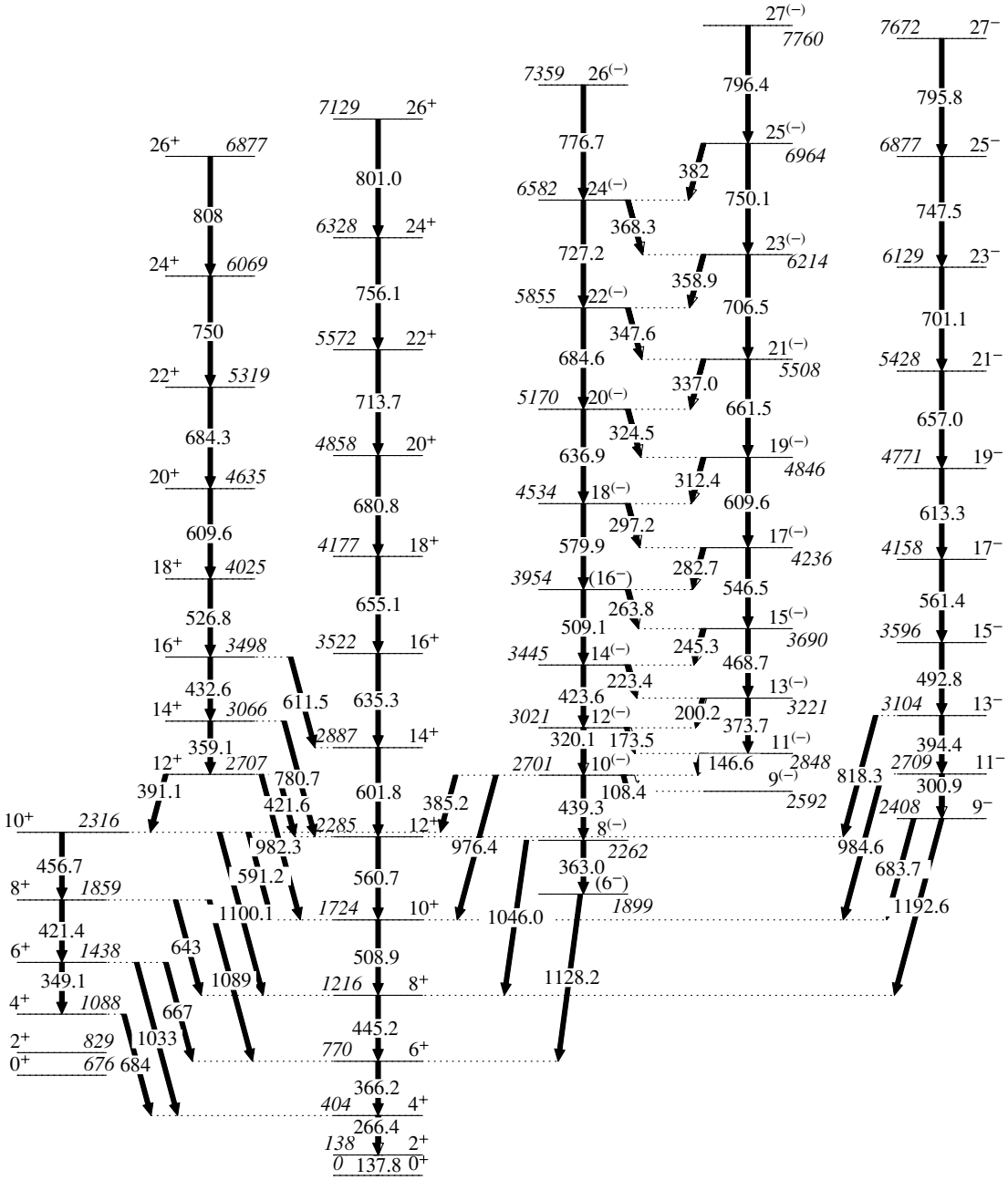

FIG. 1. Partial level scheme of ^{156}Dy according to Ref. [3].

is controlled by a feedback system using a piezoelectric device. More details about the plunger setup can be found in Ref. [18]. The target consisted of 0.9 mg/cm^2 tin, enriched to 97.7% ^{124}Sn, which was evaporated onto a 1.8 mg/cm^2 Ta foil serving as a backing. At these conditions, the energy of the ^{36}S ions after passing through the backing foil amounted in the middle of the target to 142 MeV to ensure a maximal reaction cross section. A 12.0 mg/cm^2 Au foil was used to stop the recoils leaving the target with a mean velocity $\langle v \rangle$ of 1.83(2)% of the velocity of light c. The γ rays deexciting the ^{156}Dy nuclei, which are produced in the dominant exit channel of the reaction, were registered with the GASP array [19] in its configuration I. This array consists of 40 large-volume Compton suppressed high-purity germanium (HPGe) detectors and an inner bismuth germanate (BGO) ball which in the case of our experiment consisted of 74 elements. For the data analysis, the 40 HPGe detectors were grouped into seven rings such that all detectors of one ring were positioned at approximately the same angle with respect to the beam axis. For the present coincidence RDDS experiment, the rings of interest are naturally those where appreciable Doppler shifts can be observed, namely ring 0 (mean angle with respect to the beam axis of 34.6°), ring 1 (59.4°), ring 5 (120.6°), and ring 6 (145.4°). Each of these rings consists of six detectors. As a trigger condition for data acquisition, two-fold or higher germanium signals were required to fire in coincidence with

at least two BGO elements. In the measurement, data were taken at 23 target-to-stopper distances x ranging from 2.7 to 2902 μm. In addition, data were taken at the electrical contact between the target and stopper foils, i.e., at $x \approx 0\mu$m. After corrections for energy shifts and gain matching of the detectors, the data were sorted into 1176 γ-γ coincidence matrices (4096 × 4096). To correct for random coincidences, these matrices were built by subtracting matrices constructed using a nonprompt time gate from matrices corresponding to a prompt time gate. Each final matrix accumulates coincident events where two γ rays are registered by detectors belonging to a particular two-ring combination at a given distance. A total of 2.1×10^9 doubles and higher-fold events were collected. Normalization factors for the different distances were determined by using events corresponding to pairs of strong coincident transitions (cf. also Ref. [18]). As part of the experiment, energy, full width at half maximum, and efficiency calibrations were made with an ^{152}Eu source. With the same setup, we also performed a Doppler-shift attenuation (DSA) lifetime measurement for the higher spin states, the results of which are presented in Ref. [20]. Spectra for the analysis of the RDDS data were obtained by setting a gate from above on the shifted component of a transition feeding the level of interest. Examples of such spectra at different distances are shown in Fig. 2 to illustrate the quality of the data.

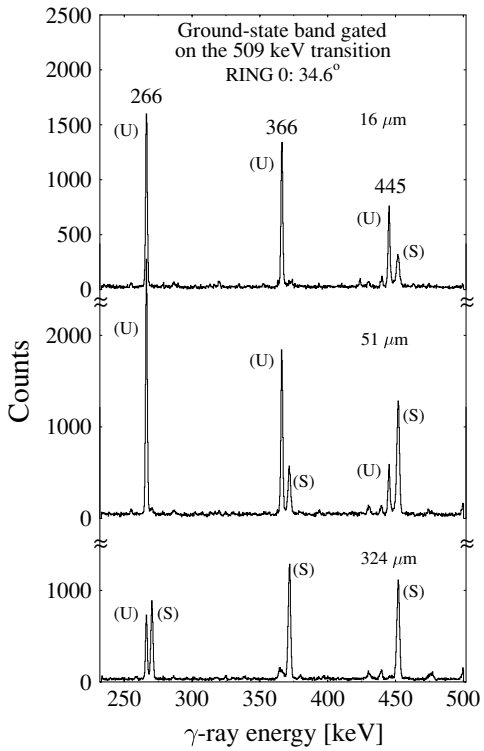

FIG. 2. Spectra of transitions in the ground-state band of ^{156}Dy obtained with a gate set on the shifted component of the 509 keV γ-ray transition in rings 0, 1, 5, and 6. The spectra are measured at the indicated distances with the detectors positioned at 34.6° (ring 0) with respect to the beam axis. The energies of the γ-ray transitions are indicated in keV. The labels U and S denote the unshifted and shifted components of the transitions, respectively.

III. DATA ANALYSIS

A. Analysis of the RDDS data

For the data analysis, the differential decay curve method (DDCM) developed in Refs. [12,13] was employed. Referring the reader for the details to the quoted works, here we only present the main points of the procedure. At each target-to-stopper distance x, the lifetime $\tau(x)$ of the level of interest is obtained from

$$\tau(x) = \frac{\{C_s, A_u\} - \alpha\{C_s, B_u\}}{\frac{d}{dx}\{C_s, A_s\}} \frac{1}{\langle v\rangle}, \tag{1}$$

where

$$\alpha = \frac{\{C_s, A_u\} + \{C_s, A_s\}}{\{C_s, B_u\} + \{C_s, B_s\}}. \tag{2}$$

Here, $\langle v\rangle$ is the mean velocity of the recoiling nuclei, and the quantities in braces are the number of coincident events corresponding to detection of the Doppler-shifted (s) or the unshifted (u) components of the γ-ray transitions involved in the analysis. In Eq. (1), it is implied that transition A depopulates the level of interest whose lifetime has to be determined and which is fed directly by transition B. The gate is set on the s component of transition C lying higher in the cascade above the level of interest, and only one feeding path leads to level A. More general expressions for the derivation of $\tau(x)$ for the case of complex feeding patterns can be found in Refs. [12,13]. In the interesting case of a gate set on the direct feeding transition B, Eq. (1) reduces to

$$\tau(x) = \frac{\{B_s, A_u\}}{\frac{d}{dx}\{B_s, A_s\}} \frac{1}{\langle v\rangle}. \tag{3}$$

The derivative in the denominator of Eqs. (1) and (3) is obtained by fitting piecewise with polynomials the gated decay curve of the shifted component of transition A (i.e., the quantities $\{C_s, A_s\}$ or $\{B_s, A_s\}$, respectively).

Obviously, the derived values of τ (the τ curve) should not depend on the distance at which they have been determined and correspondingly should be constant when plotted versus distance. A deviation from such behavior immediately indicates the presence of systematic errors in the analysis. For the derivation of the mean value of the lifetime, not all points of the τ curve are used but only those which are reliably defined, i.e., lie within the so-called region of sensitivity. Usually, this region covers the interval of distances where the quantities participating in the right-hand side of Eqs. (1) and (3) are not too small. By gating from above the level of interest, all problems related to unobserved feeders are eliminated. In addition, by gating only on the shifted component of a feeding transition, the effect of nuclear deorientation cancels out completely and does not influence the results of the lifetime analysis [21].

Figure 3 illustrates the lifetime determination for the 6_1^+ level in ^{156}Dy. The data are measured with the detectors of ring 0, and the gate is set on the shifted component of the direct feeding transition of 445 keV (cf. Fig. 1; also, for more details see Sec. IV). The areas $I_{\rm sh} = \{B_s, A_s\}$ of the shifted component of the analyzed transition of 366 keV are presented in the middle panel together with a curve corresponding to a

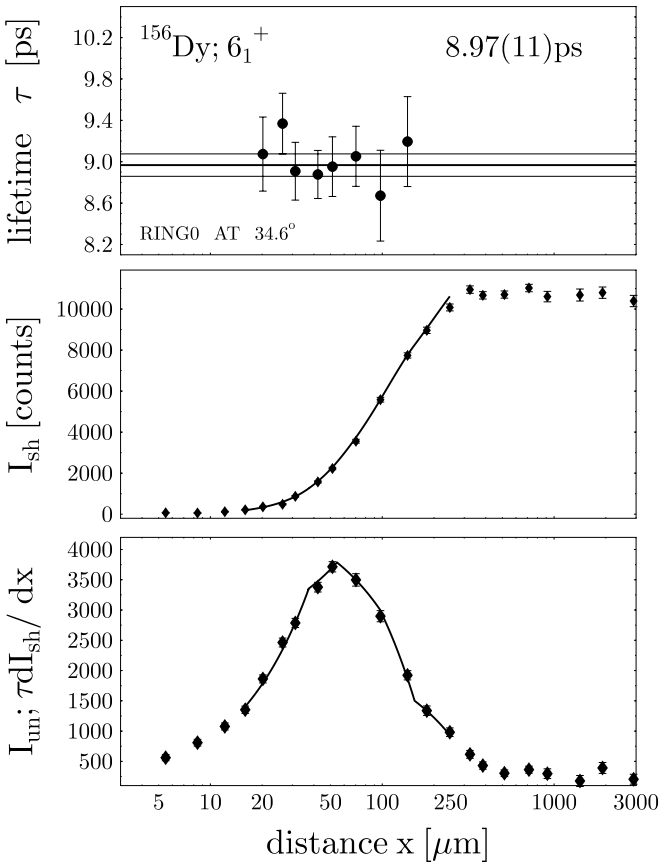

FIG. 3. Lifetime analysis at the 6_1^+ level. Middle panel shows the intensity I_{sh} of the shifted component of the 366 keV transition measured with the detectors of ring 0 in coincidence with a gate on the shifted component of the directly feeding transition of 445 keV. The curve is a piecewise polynomial fit of the shifted component; quantity I_{sh} corresponds to the quantity $\{B_s, A_s\}$ in Eq. (3). Bottom panel shows the intensity of the unshifted component I_{un} of the 366 keV transition at the same gating conditions. It corresponds to the quantity $\{B_s, A_u\}$ in Eq. (3). The curve in the bottom panel represents the derivative of the fitting function from the panel in the middle multiplied by the value of the lifetime τ derived from the analysis. This function reproduces the unshifted component, which, divided by the derivative according to Eq. (3), yields the values of the lifetime displayed in the top panel for each distance. The mean value of the lifetime and its uncertainties are also shown.

piecewise fit with second-order polynomials. The derivative of that curve as a function of distance x corresponds to the quantity $\frac{d}{dx}\{B_s, A_s\}$ in Eq. (3). The numerator $\{B_s, A_u\}$ in that equation, namely, the areas I_{un} of the unshifted peak of the 366 keV transition, is presented in the bottom panel. The values of the lifetime at each distance x obtained using Eq. (3) and which lie in the sensitivity region are displayed in the top panel. The mean value of the lifetime is also indicated with its uncertainties. The derivative $\frac{d}{dx}\{B_s, A_s\}$ of the areas of the shifted component (or $\frac{d}{dx}I_{sh}$), multiplied by the mean value of the lifetime, is displayed in the bottom panel. This curve, as it should be expected, reproduces quite well the areas of the unshifted component I_{un}. Further examples of lifetime determination can be found in the next section.

In practice, the analysis was performed by considering separately the coincidence data taken with the detectors belonging to the different rings of GASP. To investigate a given level, gates on a feeding transition were set in the γ-γ matrices at all rings where contaminants or other problems did not disturb the gated spectra. Then, the spectra corresponding to every "gated" ring at each distance x were summed up, and the resulting spectrum analyzed. With two forward and two backward rings, this means that (maximum) four lifetime values were determined for both direct and indirect feeder cases. The lifetimes determined from different matrices as well as with different gates are statistically independent and allow a check of consistency. The final value of the lifetime τ of every level of interest was derived by averaging the individual results.

A more careful consideration of the data is necessary in the cases where the lifetimes determined are comparable to or smaller than the mean slowing-down time of the ^{156}Dy ions in the gold stopper. During the slowing down, which takes place in about 1.2 ps, the emission of deexciting γ rays leads to the appearance of a complementary (DSA) component in the total line shape which can be treated according to the technique described in Ref. [22], where further details can be found. To derive correction factors for the full range of short lifetimes of interest, we applied the approach introduced in Ref. [23]. Gated spectra for the different distances were simulated, using again the results of Ref. [22], with a cascade of levels possessing properties close to the observed ones. Then, these spectra were analyzed according to the conventional DDCM, i.e., without taking into account the DSA effects. The determined lifetimes were compared to the ones implemented in the simulation, and thus a set of correction factors was derived. These correction factors increase to 43% for the shortest lifetime derived in the present work (see next section) and, on the other hand, are not needed for lifetimes larger than 2.0 ps. They were determined using stopping powers for ^{156}Dy ions in gold derived from the tables of Northcliffe and Schilling [24] with corrections for the atomic structure of the medium [25,26]. More details on our approach for the Monte Carlo simulation of the slowing down of the recoils can be found in Ref. [22] and the references cited therein.

B. Determination of branching ratios

To determine branching ratios in ^{156}Dy, we used the data from the measurement with the DSA method described in Ref. [20]. The experimental setup for this measurement was the same as for the RDDS measurement from the present work. The only difference was that the Sn material of the target (0.9 mg/cm^2) was directly evaporated onto a 13.4 mg/cm^2 Ta foil serving as a backing to stop the recoils. Branching ratios were determined in the first excited band of positive parity, for $\Delta I = 0$ and $\Delta I = 2$ transitions. For this purpose, spectra were obtained by gating on pure $E2$ transitions with $\Delta I = 2$ $(I + 2 \rightarrow I)$ which directly populate the level of interest. The gate was set in a coincidence matrix (59°, Σ) on the axis (Σ) associated with the detection of γ rays by every detector of GASP. The gated spectra were associated

with the detection of γ rays by the detectors of ring 1 at 59.4°. An efficiency correction was applied using the results of the already mentioned calibration with a ^{152}Eu source. To correct for the angular correlation effects, the following steps were performed. The 219 possible two-detector combinations in the matrix (59°, Σ) were reduced to 48 angular correlation groups by using the relations [27]

$$W(\theta_1,\theta_2,\phi)=\begin{cases} W(180^\circ-\theta_1,180^\circ-\theta_2,\phi),\\ W(\theta_1,180^\circ-\theta_2,\phi+180^\circ),\\ W(180^\circ-\theta_1,\theta_2,\phi-180^\circ),\\ W(\theta_1,180^\circ-\theta_2,180^\circ-\phi),\\ W(180^\circ-\theta_1,\theta_2,180^\circ-\phi). \end{cases} \quad (4)$$

The function $W(\theta_1,\theta_2,\phi)$ describes the angular correlation [28] of two successive γ rays, the first being detected at an angle θ_1 with respect to the beam axis and the second one being detected at an angle θ_2. The angle between the planes defined by the detection directions and the beam axis is denoted by ϕ. In our case, to minimize the number of correlation groups, the precise values of some of the polar and azimuthal angles of the GASP detectors were replaced by approximated values differing by no more than 3.4° from the actual values. Then, the angular correlation functions for the $I+2\rightarrow I\rightarrow I-2$ and $I+2\rightarrow I\rightarrow I$ cascades were calculated by averaging over the possible detector pairs participating in the building up of the matrix (59°, Σ). According to Ref. [3], the investigated $I\rightarrow I$ transitions depopulating levels in the first excited band have a pure $E2$ character. Therefore, mixing ratios $\delta_1=0$ and $\delta_2=0$ were employed in the calculation of the angular correlation functions [28]. For the transitions of interest, to characterize the distribution of the magnetic substates we employed the typical value of $\sigma=3$. Due to the specific choice of ring 1, the angular correlation effects were small, which is translated in values of the correlation function in the range 0.96–0.97 for all cascades of interest. A systematic error of 5% was added to the statistical error of the intensities determined from the efficiency corrected peak areas. The final values of the intensities, corrected for angular correlation effects, are presented in Table I. They were used for the determination of the branching ratios employed in the calculation of reduced transition probabilities.

IV. RESULTS

In the present work, 14 lifetimes have been derived, 7 in the ground-state band (g.s.b.) and 7 in the first excited band (β band at lower spins and S band at higher ones). The results of the analysis are summarized in Table II. Examples of the lifetime analysis are shown in Figs. 4–7. Below we consider in more detail the analysis of the data for the different levels investigated. These details are necessary to stress the carefulness of our analysis and to clarify discrepancies with previous experimental work.

TABLE I. Branching ratios in the first excited positive-parity band of ^{156}Dy. Data from the present work (column 4) are compared to data from [3] (column 5). n.o. denotes the nonobserved transitions.

I^π	Energy (keV)	E_γ (keV)	$I_\gamma^{\rm Exp}$	$I_\gamma^{\rm Lit}$
4_2^+	1088.3	259.6	n.o.	11(1)
		317.9	n.o.	2.0(3)
		684.1	100	100(7)
		950.5	n.o.	9.0(15)
6_2^+	1437.3	349.0	72(4)	73(4)
		666.9	100(5)	100(5)
		1033.2	14(4)	34(7)
8_2^+	1858.6	421.3	100(4)	100(7)
		642.5	40(3)	65(10)
		1089.3	12(2)	8(2)
10_2^+	2315.6	456.9	100(4)	100(4)
		591.6	11(2)	7(1)
		1100.3	11(3)	7(1)
12_2^+	2706.9	391.1	100(4)	100(6)
		421.0	61(4)	n.o.
		982.2	21(4)	43(8)
14_2^+	3065.9	178.7	n.o.	
		359.1	100(4)	
		780.0	6(2)	
16_1^+	3498.8	432.6	–	55(4)
		611.3	([a])	100(4)
18_1^+	4025.8	527.1	100	100

[a]Contaminated by the 609.6 keV transition ($20_1^+\rightarrow 18_1^+$).

A. Ground-state band

Because of the small Doppler shifts of the 266 keV transition, only the most upstream and downstream detector

TABLE II. Lifetimes determined in the present work in ^{156}Dy. The values $\tau_{\rm corr}$ are corrected for the finite slowing-down time of the recoils in the stopper. The literature values in column 5 are taken from Refs. [4,5]. See also text.

I^π	Energy (keV)	τ (ps)	$\tau_{\rm corr}$ (ps)	$\tau_{\rm Lit}$ (ps)
2_1^+	137.8	1060(150)	1060(150)	–,1187(11)
4_1^+	404.2	45.6(5)	45.6(5)	42.6(38), 43.0(40)
6_1^+	770.4	9.04(15)	9.04(15)	11.3(8), 13.2(11)
8_1^+	1215.6	3.31(10)	3.31(10)	3.2(2), 3.2(5)
10_1^+	1724.5	1.51(8)	1.69(11)	1.29(8), 1.3(3)
12_1^+	2285.2	0.90(5)	1.04(7)	0.78(5), 0.67(14)
14_1^+	2887.0	0.49(13)	0.70(15)	0.98(12), 0.73(10)
4_2^+	1088.3	6.5(17)	6.5(17)	–
6_2^+	1437.3	5.14(34)	5.14(34)	–
8_2^+	1858.6	3.02(15)	3.02(15)	–
10_2^+	2315.6	2.24(14)	2.24(14)	–
12_2^+	2706.9	6.53(15)	6.53(15)	–
14_2^+	3065.9	10.8(3)	10.8(3)	6.2(10), 7.8(8)
16_1^+	3498.8	1.87(7)	2.00(11)	–, 1.6(7)

rings (0 and 6) were used for gating in the analysis of the 2_1^+ level (cf. Fig. 1). The gated spectra were also analyzed for rings 0 and 6. Therefore, because of the long lifetime of the level, only distances above 600 μm were used.

Spectra for the analysis of the 4_1^+ level could be obtained by a gate on the direct feeding transition of 366 keV. However, there are two contaminating transitions, the $14_2^+ \rightarrow 12_2^+$ of 359 keV, and the $8^{(-)} \rightarrow (6^-)$ of 363 keV, which hinder the use of the backward rings for gating. The gated spectra could be analyzed here for all four rings with appreciable Doppler shifts.

The backward rings could also not be used for gating on the direct feeder in the case of the determination of the lifetime of the 6_1^+ level. The γ line of 439 keV of the $10^{(-)} \rightarrow 8^{(-)}$ transition cannot be separated at backward angles from the shifted component of the direct feeding transition of 445 keV. In the derivation of the areas of the depopulating transition of 366 keV, two contamination γ lines have to be taken into account. One of them (of 359 keV) originates from the decay $14_2^+ \rightarrow 12_2^+$ and influences the gated spectra only with its Doppler-shifted component. This causes difficulties in determing the areas of the transition of interest at forward rings. Another γ line of 363 keV originates from the depopulation of the $21/2^+$ level in ^{155}Dy, produced in a competing reaction channel. This level is fed indirectly by a 442 keV transition, whose shifted component cannot be strictly separated from the shifted component of the 445 keV transition. Therefore, this contamination has to be taken into account when the areas of both shifted and unshifted peaks are determined. The comparison of the lifetime values obtained by using different rings leads to a very good agreement. We should note that if we use the contaminated backward rings for gating and do not take into account the 363 keV transition, we can reproduce the result of the measurement [5] which led to a lifetime value that is 44% higher than the real lifetime. The lifetime analysis at the 6_1^+ level is illustrated for ring 0 in Fig. 3.

The lifetime of the 8_1^+ level could be determined only by using gates on indirect feeders because higher in the cascade, the $16^{(-)} \rightarrow 14^{(-)}$ transition has exactly the same energy (509 keV) as the direct feeding transition (cf. Fig. 1). Although the contaminating intensity is weak, it leads to the appearance of a long-lived component in the quantities describing the time behavior of the 8_1^+ level. Therefore, we used for gating the 602 keV $14_1^+ \rightarrow 12_1^+$ transition at ring 5. At forward angles, the gates were contaminated by the $20_1^+ \rightarrow 18_1^+$ transition of 609 keV. Ring 6 could not be used because of the $10_2^+ \rightarrow 10_1^+$ transition of 591 keV. All other higher-lying γ lines in the ground-state band were contaminated by transitions within the bands of negative parity. In the spectra gated by the indirect feeder, the areas of the depopulating transition of 445 keV and of the direct feeder of 509 keV transition have been determined. In the latter case, the influence of the annihilation line of 511 keV, which was not fully suppressed by the sorting procedure, had to be taken into account. The analysis at all four gated rings yielded consistent results. The lifetime analysis at the 8_1^+ level is illustrated for ring 1 in Fig. 4.

In the determination of the lifetime of the 10_1^+ level, the direct feeding transitions were weak (interband) or contaminated. The direct feeding transition of 561 keV in the ground-state band overlaps with the $17_1^- \rightarrow 15_1^-$ transition. With the same arguments for the choice of gates, the same gated spectra as for the 8_1^+ level were used here. The areas of the 509 keV transition were simply taken from the analysis of the lower level. To determine the areas of the 561 keV transition, it was necessary to take into account in rings 0 and 6 a contamination originating from ^{155}Dy. The contaminating γ line of 550 keV belongs to the $(23/2^-) \rightarrow 19/2^-$ transition and is fed by a transition of 593 keV. The γ line of the latter transition lies in the spectrum measured with ring 5 at the same place as the shifted component of the transition used for gating. Again the lifetime values obtained at the four gated rings were in very good agreement.

The lifetime of the 12_1^+ level could be determined by using a directly feeding transition for the gate in rings 5 and 6. At forward angles, the shifted component of the direct feeder is contaminated by the transitions $20_1^+ \rightarrow 18_1^+$ of 610 keV and $16_1^+ \rightarrow 14_1^+$ of 611 keV. The areas of the depopulating transition of the 561 keV transition were determined by taking into account the contamination of the γ line from ^{155}Dy (cf. above, lifetime determination at the 10^+ level). The results obtained at the four rings analyzed are in a good agreement.

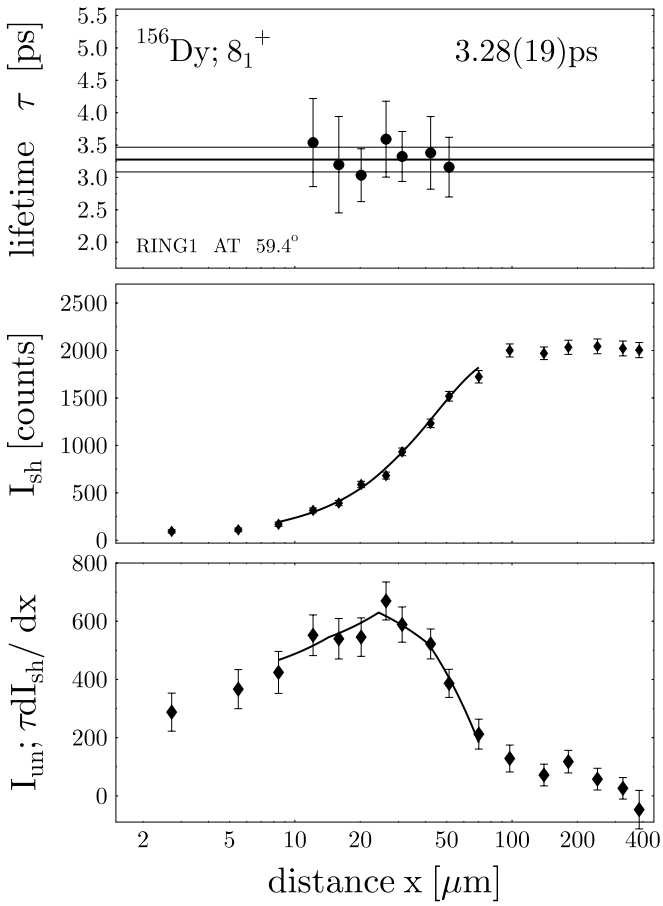

FIG. 4. Same as in Fig. 3, but for the 8_1^+ level using a gate set on an indirect feeder. Here the bottom panel shows the numerator of Eq. (1).

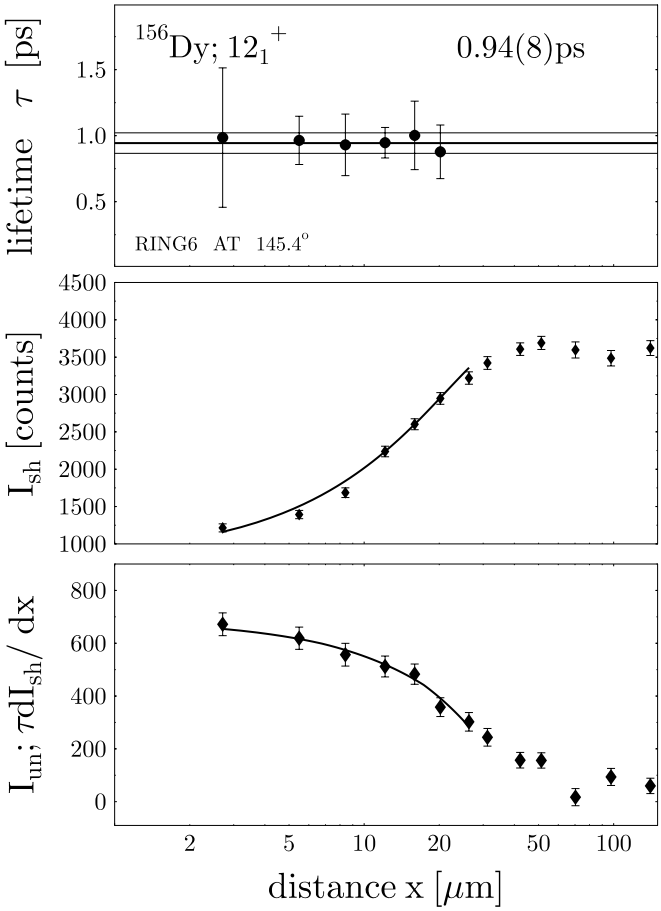

FIG. 5. Same as in Fig. 3, but for the 12_1^+ level.

The lifetime analysis at the 12_1^+ level is illustrated for ring 6 in Fig.5.

Due to the short lifetime of the 14_1^+ level, only the data measured at the shortest distances could be used for its determination. Contaminating transitions were not present in the gates nor in the gated spectra to be analyzed. This allowed the use of the full statistics of all rings.

The results of the analysis are presented in Table II where they are compared to earlier data [4,5] for ^{156}Dy. As already mentioned, the finite slowing-down time of the recoils in the stopper influences the determination of the short lifetimes (below 2 ps in the present case). The values determined using our standard approach were corrected for this effect according to the procedure outlined in Ref. [23] and are labeled as τ_{corr} in Table II. Compared with data from the literature for the g.s.b., the present shorter value of the 6_1^+ level is impressive. With the exception of the case of the 2_1^+ level, the lifetimes from the present work are characterized by smaller uncertainties.

B. First excited band

The long lifetimes of the 12_2^+ and 14_2^+ levels lead to a long effective feeding time for the states below the band crossing. An additional problem that appears in the analysis of this band is the leak of intensity to the g.s.b. levels. Because of the latter effect, the lowest level in the first excited band whose lifetime could be determined is the 4_2^+ one.

To derive its lifetime, gates were set on the directly feeding transition of 349 keV in all four rings. The only observed decay of the 4_2^+ level is through the transition of 684 keV to the 4_1^+ level. Nevertheless, the statistics of only one gated ring were not sufficient for a determination of the area of the unshifted component. To obtain a suitable signal for this component, it was necessary to add the spectra measured at different angles. For this purpose, the spectrum in the region of interest where the two components are separated was divided into two parts, each containing one of the components. The spectrum containing the shifted component was shifted to coincide with the shifted component in ring 0. The shifted components measured with the detectors at backward angles were reflected with respect to the mean position of the distribution of the unshifted peaks. A complementary difficulty in the analysis was caused by contamination from the $22_1^+ \rightarrow 20_1^+$ transition in the S band higher in the cascade. This contamination appears only in the shifted component of the spectrum of the investigated $4_2^+ \rightarrow 4_1^+$ transition of 684 keV. The 22_1^+ level has a very short lifetime ($\tau = 0.4$ ps), and in the spectra for the distances of importance ($x \geqslant 70\,\mu$m) in deriving the lifetime of the 4_2^+ level, the full intensity of the $22_1^+ \rightarrow 20_1^+$ γ line is Doppler shifted. Its contribution to the shifted-peak area of the 684 keV transition could be determined, after an efficiency and intensity balance correction, from the intensity of the $18_1^+ \rightarrow 16_1^+$ transition and correspondingly subtracted. It was found that about 65% of the area of the investigated shifted peak is due to the contamination.

For the 6_2^+ and 8_2^+ levels, the gates on the direct feeding transition could be employed without problems from contamination. Similarly, no contamination was present in the gated spectra at all four rings.

The gate on the 391 keV transition, which directly populates the 10_2^+ level, is contaminated at backward angles by the $10^{(-)} \rightarrow 10_2^+$ transition of 385 keV. Therefore, only rings 0 and 1 were used for gating. For the analysis of the depopulating γ line of 457 keV, all four rings were employed.

For the 12_2^+ level, again gates on the direct feeding transition could be employed with the exception of ring 0. In this ring, the shifted component of the direct feeder is contaminated by the 366 keV transition in the g.s.b. (cf. Fig. 1). The results in the four analyzed gated rings are in good agreement. The analysis for the 12_2^+ level at ring 5 is illustrated in Fig. 6.

When setting the direct gates for the analysis of the 14_2^+ level, it was necessary to take into account the contaminating cascade $10^{(-)} \rightarrow 8^{(-)} \rightarrow (6^-)$ consisting of the transitions of 439 and 363 keV. This contamination could be avoided by using gates in rings 5 and 6. To analyze the depopulating 359 keV transition, it was necessary to take into account the presence of the transition $6_1^+ \rightarrow 4_1^+$ of 366 keV. The analysis for the 14_2^+ level at ring 6 is illustrated in Fig. 7.

To analyze the data for the 16_1^+ level by gating on the directly feeding transition, it was necessary to avoid a contamination originating from ^{155}Dy. Gates set at the forward rings provided spectra that could be analyzed in all four gated rings.

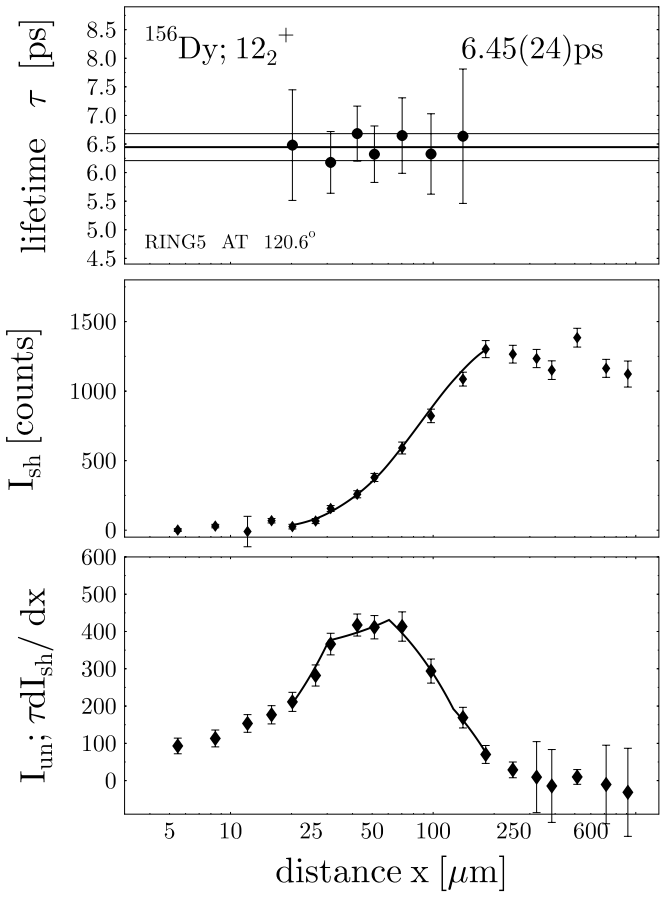

FIG. 6. Same as in Fig. 3, but for the 12_2^+ level.

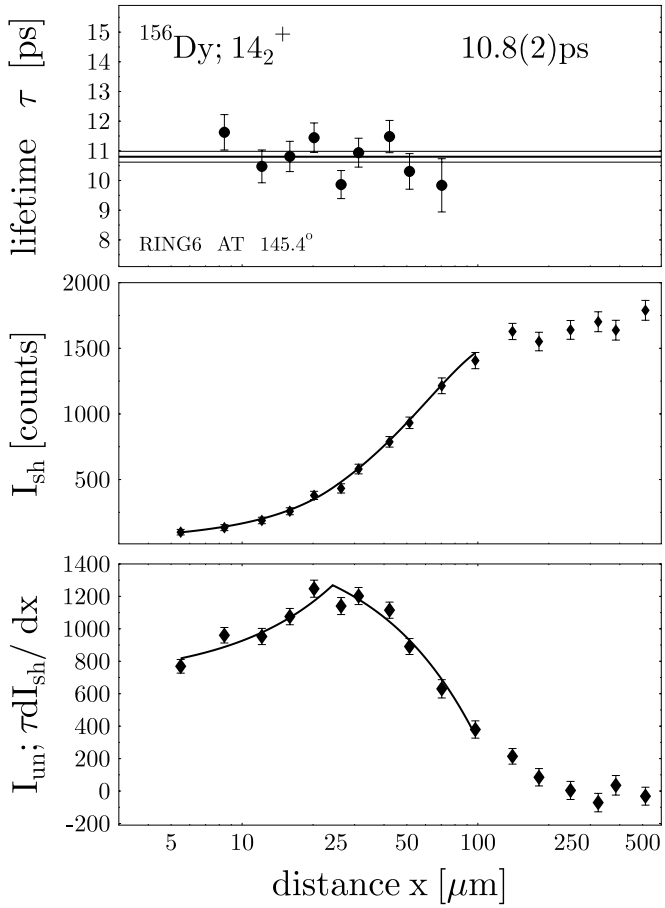

FIG. 7. Same as in Fig. 3, but for the 14_2^+ level.

The results of the analysis for the first excited band are summarized in Table II. Almost all level lifetimes are determined for the first time. The lifetimes of the 14_2^+ and 16_1^+ levels are longer than the earlier determined values [4,5].

The reduced electromagnetic transition probabilities $B(E2)$ derived in this work are presented in Table III.

V. DISCUSSION

In Fig. 8, we present the transition quadrupole moments Q_t in the g.s.b. derived from the experimental $B(E2)$ values using the relation

$$B(E2, I \to I-2) = \frac{5}{16\pi} Q_t^2 \langle I K 20 | I-2K \rangle^2, \qquad (5)$$

with $K = 0$. In the framework of the rigid-rotor model [29], the transition quadrupole moments within a band are equal to the intrinsic quadrupole moment Q_0 which is related [30] to the deformation β via

$$Q_0 = \frac{3}{\sqrt{5\pi}} Z R_0^2 \beta (1 + 0.16\beta). \qquad (6)$$

According to Ref. [31], because of the difference between the nuclear charge distribution and the mean field, $\beta \approx 1.1\beta_{\text{mean-field}}$. The experimental Q_t values in Fig. 8 are compared to calculations performed in the framework of different nuclear models. The simplest of them is the axially symmetric rigid-rotor model [29]. The data are very well described by this model, and earlier suggestions for rotation-induced shape changes [5] are not confirmed by the present data. From the transition strength $B(E2, 2_1^+ \to 0_1^+) = 0.834\ (137)\ e^2\,b^2$, we derive $Q_0 = 6.5\ (5)\ e$b and $\beta_{\text{mean-field}} = 0.27(2)$. The experimental Q_t value for the $2_1^+ \to 0_1^+$ transition was used as a normalization factor for the theoretical calculations presented in Fig. 8. Many theoretical calculations of transition strengths within the g.s.b. up to spin $14\hbar$ and higher in the yrast band are available in the literature [8–11,32–34]. For Fig. 8, we have chosen, on the one hand, the three benchmark models—the axial rigid rotor, the X(5), and the U(5) limit of the interacting boson approximation (IBA)—which trace the gross features of the spherical to deformed phase transition. On the other hand, we show two calculations (labeled A and B) with semimicroscopic mean-field approaches which reproduce the data within the error bars. Curve A represents the cranked Hartree-Fock-Bogoliubov calculations with variation after exact projection onto good particle number from Ref. [8]. These calculations give an overall description of the level energies and predict a behavior of the $B(E2)$'s which is very close to the expectations for a symmetric rigid rotor. At higher spins in the yrast band, however, the calculations cannot reproduce the fine structure of the $B(E2)$ data, especially the fluctuations around the band-crossing region. Curve B

TABLE III. Reduced electromagnetic transition probabilities $B(E2)$ derived in this work. Column 1 displays the level spin and parity. The level and depopulating transition energies are shown in the next two columns followed by the relative γ intensity of the transitions. The multipolarity $\sigma\lambda$ of the transition and the adopted lifetime are shown in columns 5 and 6, respectively. The last two columns present the $B(E2)$ data in e^2 fm^4 and in Weisskopf units. Uncertainties are shown in parentheses.

I^π	Energy (keV)	E_γ (keV)	I_γ	$\sigma\lambda$	τ (ps)	$B(E2)$ (e^2 fm^4)	$B(E2)$ (W.u.)
2_1^+	137.8	137.8	100	$E2$	1060(150)	8340^{+1370}_{-1030}	167^{+28}_{-21}
4_1^+	404.2	266.4	100	$E2$	45.6(5)	12200(130)	245(3)
6_1^+	770.4	366.2	100	$E2$	9.04(15)	13230(220)	265(4)
8_1^+	1215.6	445.4	100	$E2$	3.31(10)	13780^{+430}_{-400}	276(9)
10_1^+	1724.5	508.9	100	$E2$	1.69(11)	13900^{+970}_{-950}	278^{+16}_{-14}
12_1^+	2285.2	560.7	100	$E2$	1.04(7)	14000^{+1000}_{-880}	281^{+20}_{-18}
14_1^+	2887.0	601.8	100	$E2$	0.70(15)	14630^{+4000}_{-2580}	293^{+80}_{-52}
4_2^+	1088.3	259.6	11(1)	$(E2)$	6.5(17)	9450^{+3500}_{-2210}	189^{+70}_{-44}
		317.9	2.0(3)	$E2$		620^{+240}_{-160}	$12.5^{+4.9}_{-3.3}$
		684.1	100(7)	$E2/E0$		680^{+250}_{-150}	$13.6^{+5.0}_{-3.1}$
		950.5	9.0(15)	$E2$		12^{+5}_{-3}	$0.24^{+0.09}_{-0.06}$
6_2^+	1437.3	349.0	72(4)	$E2$	5.14(34)	11640^{+1150}_{-1080}	233^{+23}_{-22}
		666.9	100(5)	$E2/E0$		630(60)	12.7(12)
		1033.2	14(4)	$E2$		10(3)	0.20(6)
8_2^+	1858.6	421.3	100(4)	$E2$	3.02(15)	13160^{+980}_{-940}	264(19)
		642.5	40(3)	$E2/E0$		640(60)	$12.8^{+1.3}_{-1.2}$
		1089.3	12(2)	$E2$		14(2)	0.27(5)
10_2^+	2315.6	456.9	100(4)	$E2$	2.24(14)	14750^{+1320}_{-1230}	296^{+26}_{-25}
		591.6	11(2)	$E2/E0$		450(90)	8.9(18)
		1100.3	11(3)	$E2$		20(6)	0.40(11)
12_2^+	2706.9	391.1	100(4)	$E2$	6.53(15)	7320(440)	147(9)
		421.0	61(4)	$(E2/E0)$		3090(240)	62(5)
		982.2	21(4)	$E2$		15(3)	0.31(6)
14_2^+	3065.9	359.1	100(4)	$E2$	10.8(3)	11520(740)	231(15)
		780.0	6(2)	$(E2)$		14(5)	0.29(10)
16_1^+	3498.8	432.6	55(4)	$E2$	2.00(11)	9430(930)	189(19)
		611.3	100(4)	$E2$		3040(240)	61(5)

represents the calculations of Bhatt *et al.* [11] who recently investigated the wave functions of the yrast states of even-even nuclei and, in particular, of ^{156}Dy in terms of quadrupole collective states of nucleons occupying natural and unnatural parity orbitals. This work predicts a trend for a reduction of the collectivity with increasing spin after $I^\pi = 20^+$ in the yrast band (see also Ref. [20]).

The transition quadrupole moments within the first excited band and the S band are shown in Fig. 9. Around $I = 12\hbar$, the first excited band crosses with the S band [a $\nu(i_{13/2})^2$ quasiparticle band] which becomes yrast at the $I^\pi = 16^+$ level (cf. Fig. 1). The band crossings are reflected in the reduction of the Q_t values in the spin range I = 12–16$\hbar$. The experimental data are compared to the values characterizing a rigid rotor with the same deformation as the g.s.b. and to the values inherent in the first excited band ($S2$) in the X(5) model (in the spin range $I = 4 - 10\hbar$). At spin $I = 22\hbar$ and above, the experimental values from Ref. [20] are also shown. Two features immediately emerge. First, a rigid-rotor description with a slightly smaller deformation than that of the g.s.b. (i.e., $Q_t \approx 6.2\,e$ b) is able to reproduce the data with the exception of the band-crossing region. Second, although the error bars are large to allow a final conclusion, the experimental Q_t values at lower spins are rather well reproduced by the X(5) model. This fact is in contrast with the observations for the g.s.b. and therefore suggests a possible coexistence of an

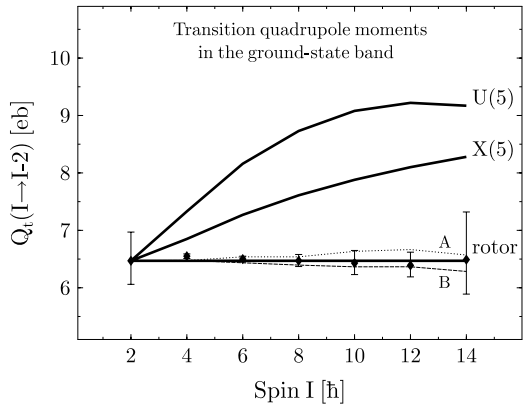

FIG. 8. Transition quadrupole moments Q_t in the ground-state band of ^{156}Dy. The measured values are compared against the expected ones for a rigid rotor, an X(5)-like nucleus, and the U(5) limit of the IBA as well as calculations from Ref. [8] (curve A) and Ref. [11] (curve B).

X(5)-like structure of the first excited band and a g.s.b. that does not possess X(5) properties. In the following discussion, we concentrate on the clarification of the position of ^{156}Dy in the transitional region between spherical and deformed nuclei.

In the case of the X(5) critical point symmetry, which describes the spherical to axially deformed phase transition, the collective nuclear potential is approximated by a square well and a harmonic oscillator potential with respect to the β and γ degrees of freedom, respectively. In addition, the β and γ degrees of freedom are considered to be decoupled. The corresponding Hamiltonian can then be solved analytically, and specific predictions can be made for both the energy spectrum and the transition probabilities [14]. The X(5) energies of the lowest band ($S1$) are located between the vibrator and symmetric rotor values. As shown in [35], the g.s.b. energies normalized to the 2^+ band member of the $N = 90$ isotones ^{150}Nd, ^{152}Sm, ^{154}Gd, and ^{156}Dy follow the X(5) predictions very well. Crucial observables

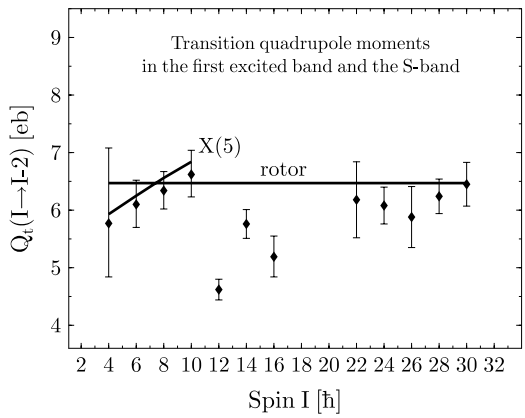

FIG. 9. Transition quadrupole moments Q_t in the first excited band and the S band of ^{156}Dy. Measured values are compared with the expected ones for an X(5)-like nucleus and a rigid rotor with the g.s.b. deformation. For spins above $20\hbar$, the data from the measurement described in Ref. [20] are shown.

TABLE IV. Comparison of energy ratios of several $N = 90$ nuclei with the X(5) values.

Energy ratio	^{150}Nd	^{152}Sm	^{154}Gd	^{156}Dy	X(5)
$R(4/2)_{S1}$	2.93	3.01	3.01	2.93	2.91
$R(4/2)_{S2}$	2.63	2.69	2.71	2.67	2.80
$R(0_{S2}/2_{S1})$	5.19	5.62	5.53	4.90	5.67
$R(2_{S2}/2_{S1})$	1.35	1.03	1.10	1.11	1.81

are also the energy ratios

$$R(4/2)_{S1} = E(4_1^+)/E(2_1^+),$$
$$R(4/2)_{S2} = [E(4_2^+) - E(0_2^+)]/[E(2_2^+) - E(0_2^+)],$$
$$R(0_{S2}/2_{S1}) = E(0_2^+)/E(2_1^+),$$
$$R(2_{S2}/2_{S1}) = [E(2_2^+) - E(0_2^+)]/E(2_1^+).$$

The data in Table IV clearly show that for the considered $N = 90$ isotones, these quantities also agree well with the X(5) values. An overall exception is the energy spacing in the $S2$ band $[R(2_{S2}/2_{S1})]$ as well as the position of the $S2$ bandhead in ^{156}Dy. Nevertheless, the nuclei ^{150}Nd [16], ^{152}Sm [15], ^{154}Gd [17] have been found to represent very good examples of the realization of the X(5) symmetry. Therefore, it is of special interest to determine in more detail for ^{156}Dy the extent to which the electromagnetic transition probabilities determined in this work can be reproduced by the X(5) predictions.

An important criterion for comparison are the relative $B(E2)$ transition strengths of the transitions depopulating levels of the first excited band ($S2$). Table V compares the experimental values from Ref. [35] and the present work to the X(5) values. Although there exist differences between theory and experiment, there is a tendency toward an overall agreement. We recall that the experimental Q_t values within the g.s.b. do not agree with the X(5) model, while those in the first excited band follow the X(5) predictions. Therefore, one can characterize the result of the comparison of the experiment

TABLE V. Relative $B(E2)$ values for some levels of the first excited band in ^{156}Dy. Experimental values from the present work and the literature are compared to X(5) predictions.

Transition	$B(E2)^{\mathrm{rel}}$		
	X(5)	Ref. [35]	Exp.
$2_2^+ \to 0_1^+$	3	<0.1	
$\to 2_1^+$	11	7.7(4)	
$\to 4_1^+$	46	10.0(5)	
$\to 0_2^+$	100	<100	
$4_2^+ \to 2_1^+$	1	0.12(2)	
$\to 4_1^+$	5	7(1)	
$\to 6_1^+$	23	7(1)	
$\to 2_2^+$	100	100(10)	
$6_2^+ \to 4_1^+$	0.5	0.20(4)	0.08(2)
$\to 6_1^+$	3	5.4(3)	5.4(3)
$\to 8_1^+$	15	<79	n.o.
$\to 4_2^+$	100	100(5)	100(5)

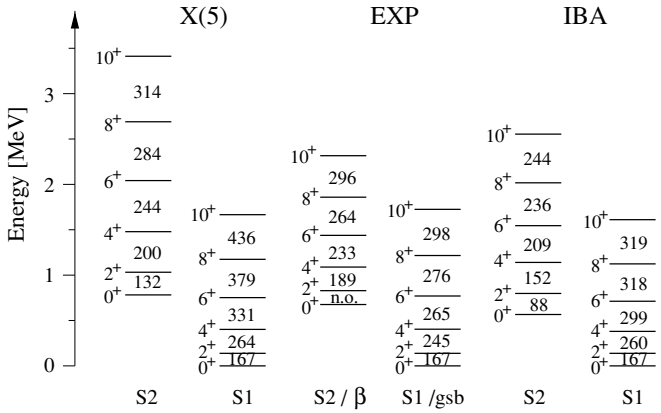

FIG. 10. Comparison of level energies and $B(E2)$ transition strengths (in W.u.) of ^{156}Dy with the X(5) and IBA predictions. $B(E2; 2_1^+ \rightarrow 0_1^+)$ model values are normalized to the experimental data.

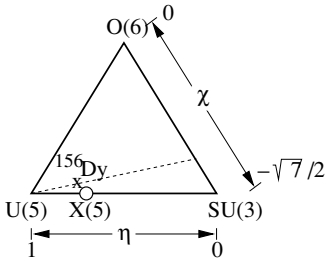

FIG. 11. Casten triangle for parameters of IBA-1. Position of ^{156}Dy nucleus is indicated.

and the X(5) model as a partial agreement. At this point, however, it should be again mentioned that the X(5) does not use fitting parameters and has only two scaling parameters for the energies and the $B(E2)$ values.

To obtain a better theoretical description of ^{156}Dy, we employed the IBA-1 model [36]. For this purpose, we used the two-parameter Hamiltonian [37]

$$\hat{H}(N, \eta, \chi) = \eta \hat{n}_d + \frac{\eta - 1}{N} \hat{Q}_\chi \cdot \hat{Q}_\chi, \tag{7}$$

with the operator of the number of d bosons $\hat{n}_d = d^\dagger \cdot \tilde{d}$ and the scalar product of the quadrupole operators

$$\hat{Q}_\chi = [d_\mu^\dagger s + s^\dagger \tilde{d}_\mu]^{(2)} + \chi [d_\mu^\dagger \times \tilde{d}_\mu]^{(2)}. \tag{8}$$

With 8 valence neutrons and 16 valence protons, the number of bosons in ^{156}Dy is $N = 12$. The results of the fit are presented in Fig. 10 together with the expectations of the X(5) model. The theoretical energies of the 2_1^+ level and $B(E2, 2_1^+ \rightarrow 0_1^+)$ transition strength are normalized to the experimental values. The description of ^{156}Dy by the IBA fit is quite good. Experimental energies and intraband $B(E2)$ values are satisfactorily reproduced, and the agreement found is better than the one for X(5), at the price of two additional parameters. This holds true also for the interband transition strengths. Their experimental values are compared to the theoretical ones in Table VI. Here we mention one specific difference to the expectations of the X(5) symmetry where the interband transition strengths for the $I_{S2} \rightarrow (I+2)_{S1}$ transitions are larger than for the $I_{S2} \rightarrow I_{S1}$ ones, and the $I_{S2} \rightarrow (I-2)_{S1}$ transition strengths are one order of magnitude smaller than the latter ones. This specific behavior of the interband transitions is not observed in ^{156}Dy. Here the transition probabilities of the $I_{S2} \rightarrow I_{S1}$ transitions are strongest, whereas the $I_{S2} \rightarrow (I+2)_{S1}$ ones are a bit weaker or have not been observed.

Now it is possible to compare the parameters of the present IBA fit to the parameters which best describe the X(5) symmetry. In Fig. 11, we show the Casten triangle which corresponds to the definition space of the parameters η and χ [cf. Eq. (7)]. The cross indicates the position of ^{156}Dy in this parameter space ($\eta = 0.8$, $\chi = -0.8\sqrt{7}/2$). This nucleus is very close to the critical point of X(5), here indicated by the corresponding first-order phase transitional point on the U(5)-SU(3) axis ($\eta = 0.75$, $\chi = \sqrt{7}/2$), but it deviates somewhat toward O(6) from the line interconnecting U(5) and SU(3). In other words, the role of triaxiality (γ degree of freedom) is enhanced in ^{156}Dy compared to the nuclei exhibiting the X(5) critical point symmetry. This is consistent with the fact that the γ band of ^{156}Dy is found to be lower in energy than that of the $N = 90$ isotones ^{150}Nd, ^{152}Sm, and ^{154}Gd, all of which are closer to the critical point of the X(5) symmetry. The importance of the γ degree of freedom in these transitional nuclei, and in particular of the β-γ coupling, has been recently confirmed by the work of Caprio [38], who performed precise numerical solution of the X(5) Hamiltonian without resorting to the approximations of Ref. [14].

A possibility for investigating the role of the collective degrees of freedom β and γ is provided by the General collective model (GCM). The Hamiltonian of the model, expressed in terms of invariant products of the collective quadrupole variables $\alpha_{2\mu}$, which parametrize the nuclear surface in the center of mass system, and their conjugate

TABLE VI. Comparison of the interband $B(E2)$ transition strengths (W.u.) in ^{156}Dy with the X(5), IBA, and GCM predictions.

I_{S2}	0	2			4			6			8			10	
$\longrightarrow I_{S1}$	2	0	2	4	2	4	6	4	6	8	6	8	10	8	10
Exp.	n.o.		n.o.		0.2	14	13	0.2	13	n.o.	0.3	13	n.o.	0.4	8.9
X(5)	105	3	14	60	2	10	47	1	8	37	1	7	29	1	6
IBA	91	0.7	28	17	0	21	11	0	18	7.5	0	15	5.5	0	13
GCM	61	0.1	21	20	<0.1	19	17	<0.1	19	14	<0.1	18	13	0.1	17

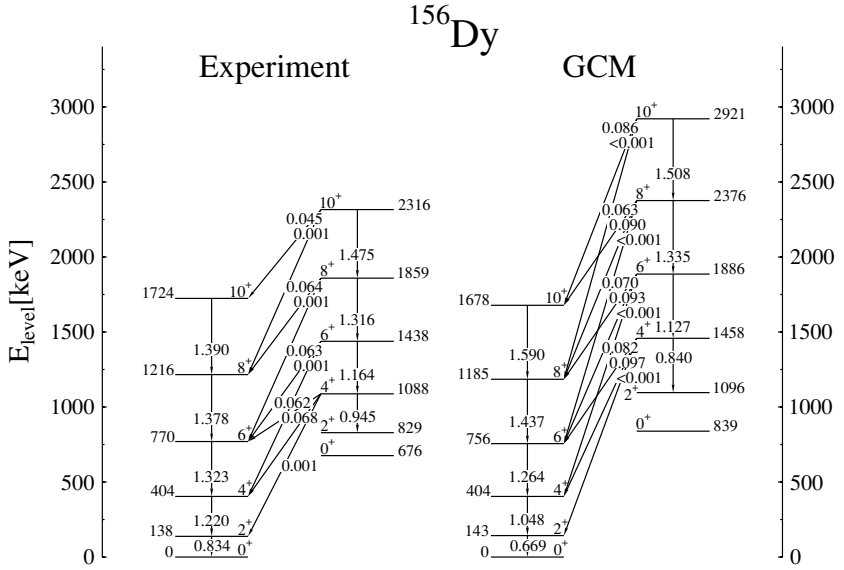

FIG. 12. Experimental level scheme and $B(E2)$ transition strengths (in $e^2\,b^2$) compared to the GCM fit.

momenta $\hat{\pi}_{2\mu}$, reads [39]

$$H = \hat{T} + V, \tag{9}$$

where

$$\hat{T} = \frac{1}{2B_2}\,[\hat{\pi} \times \hat{\pi}]^{[0]} + \frac{P_3}{3}\{[[\hat{\pi} \times \alpha]^{[2]} \times \hat{\pi}]^{[0]}\} \tag{10}$$

is the operator of the kinetic energy. A transformation to the intrinsic (body-fixed) system leads to a formal separation of the rotational and vibrational variables, expressed by the Euler angles and the shape variables β and γ, respectively. In the intrinsic system, the potential V is given by

$$\begin{aligned} V(\beta,\gamma) = {} & \frac{1}{\sqrt{5}}C_2\beta^2 - \sqrt{\frac{2}{35}}C_3\beta^3\cos 3\gamma + \frac{1}{5}C_4\beta^4 \\ & - \sqrt{\frac{2}{175}}C_5\beta^5\cos 3\gamma \\ & + \frac{2}{35}C_6\beta^6\cos^2 3\gamma + \frac{1}{5\sqrt{5}}D_6\beta^6. \end{aligned} \tag{11}$$

We performed calculations using the code developed by Troltenier *et al.* [40] with the aim of reproducing the spectroscopic properties of ^{156}Dy and deriving information on the collective potential $V(\beta,\gamma)$. The best fit of the level scheme and the $B(E2)$ transition strengths was obtained with the following set of model parameters: $B_2 = 55.7 \times 10^{-42}$ MeVs^2, $P_3 = 0.075 \times 10^{42}$ MeV^{-1} s^{-2}, $C_2 = -151.5$ MeV, $C_3 = 247.5$ MeV, $C_4 = 2580.0$ MeV, and $D_6 = 2059.5$ MeV. The results of the fit are presented in Fig. 12. The agreement with the data is quite good, with the exception of the energy spacings in the first excited band. However, these spacings are difficult to reproduce by other collective models also (see Fig. 10). The absolute $B(E2)$ transition strengths are overall well described. Thus, the interband transitions are reproduced with differences not exceeding a factor of 2 for the strong transitions (Table VI). In Fig. 13, we compare the GCM potentials derived in the present work for ^{156}Dy and in Ref. [17] for ^{154}Gd. They are similar, but nevertheless some differences exist. For instance, in the case of ^{154}Gd, the potential is more expanded in β, but the depth of the potential is larger in ^{156}Dy. This is consistent with the more rotational-like behavior of the transition strengths in the g.s.b. of ^{156}Dy compared to ^{154}Gd. The γ dependences of the two potentials, as illustrated by the bottom panels, are also similar with a somewhat larger prolate-oblate energy difference in the case of ^{156}Dy. So we may conclude that the larger potential depth can be associated with the differences in the properties of the first two excited bands in ^{156}Dy compared to the neighboring $N = 90$ nuclei ^{150}Nd, ^{152}Sm, and ^{154}Gd, in which the first two excited bands exhibit an X(5) character. With the wave functions resulting from the diagonalization of the GCM Hamiltonian, it is possible to calculate for each state $\beta_{\rm rms} = \sqrt{\langle\beta^2\rangle}$ and the average γ defined by $\langle\gamma\rangle = \frac{1}{3}\arccos(\langle\beta^3\cos(3\gamma)\rangle/\beta^3_{\rm rms})$. The widths of the distributions of these quantities, σ_β and σ_γ, respectively, can also be calculated according to the formulas given in Ref. [41]. The mean shape parameters characterizing the first two 0^+ states in ^{156}Dy and ^{154}Gd are presented in Table VII. They illustrate the properties of the wave functions corresponding to the potentials in Fig. 13. The mean characteristics of the nuclear shape in ^{156}Dy and ^{154}Gd are quite similar, with the exception of the different values of $\beta_{\rm rms}$. Although $\beta_{\rm rms}$ is larger in ^{154}Gd than in ^{156}Dy, the deeper potential in the latter nucleus, as already mentioned, seems to lead to a more rotor-like behavior of the transition strengths in the ground-state band. This fact indicates that a good rotor is characterized not only by a considerable value of β at the potential minimum but also by a sufficiently deep potential.

TABLE VII. Mean shape parameters of first two 0^+ states in ^{156}Dy and ^{154}Gd.

Nucleus	Level	$\beta_{\rm rms}$	σ_β	$\langle\gamma\rangle$	σ_γ
^{156}Dy	0^+_1	0.274	0.047	20.01°	9.35°
	0^+_2	0.266	0.071	20.56°	12.91°
^{154}Gd	0^+_1	0.306	0.055	21.22°	9.51°
	0^+_2	0.302	0.080	21.18°	12.63°

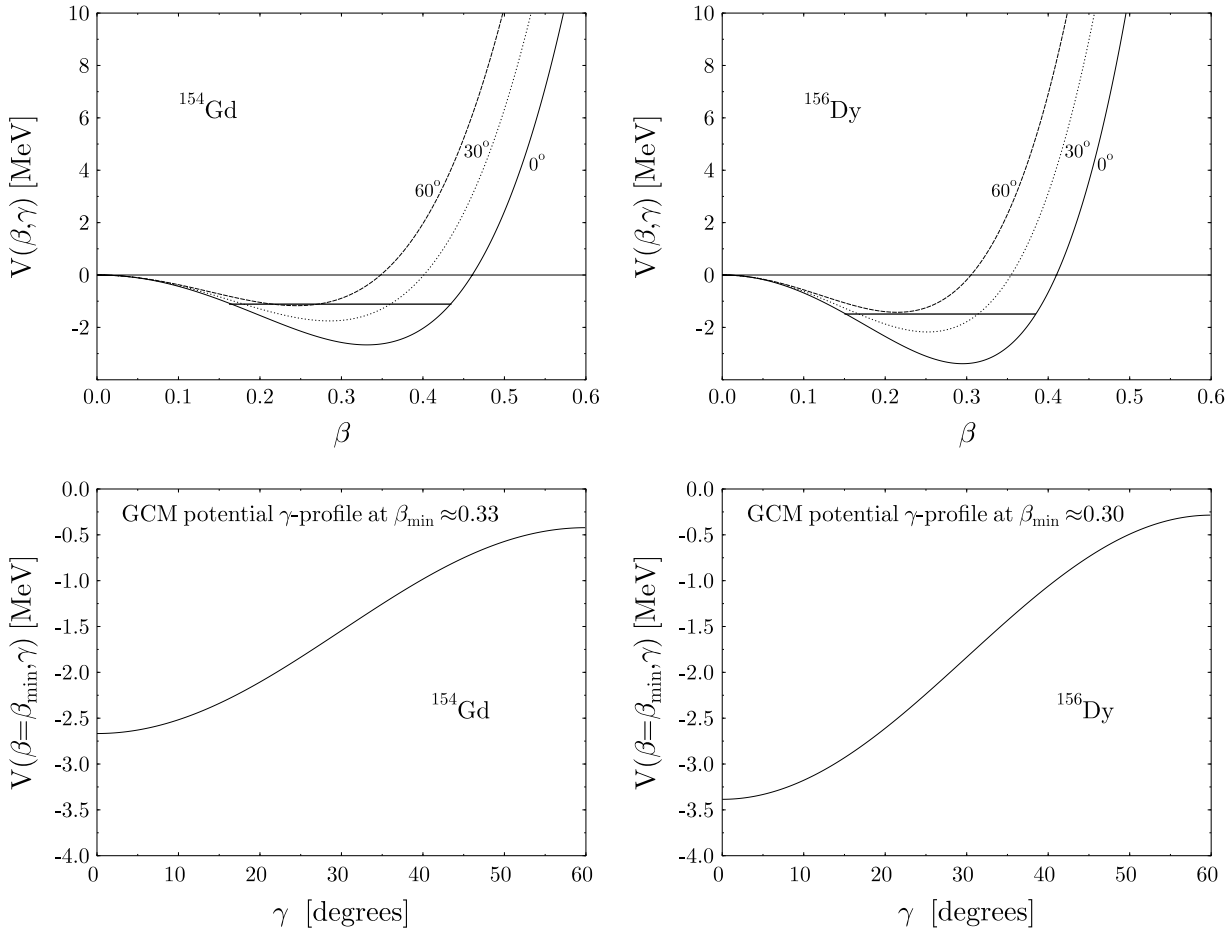

FIG. 13. GCM potentials $V(\beta, \gamma)$ for ^{156}Dy and ^{154}Gd. Top panels: projections of potentials for $\gamma = 0°$, $30°$, and $60°$. Positions of the ground states are indicated by thicker lines. Bottom panels: γ dependence of potentials at β values corresponding to coordinates of the absolute potential minimum.

The smaller width $\sigma_\beta = 0.047$ characterizing the ground state of ^{156}Dy points again to the fact that this nucleus is a better rotor than ^{154}Gd [$\sigma_\beta(0_1^+) = 0.055$]. It is also interesting to compare the mean shape parameters of the 0_1^+ and 0_2^+ states in the same nucleus. Their values are quite close to each other, but some slight differences exist, especially in the widths of the distributions σ_β and σ_γ.

VI. SUMMARY AND CONCLUSIONS

Precise and reliable lifetimes of excited states in ^{156}Dy were measured using the coincidence RDDS technique at the GASP multidetector array. New values for the γ-ray branching ratios for transitions depopulating levels of the first excited band were derived. Shape changes previously suggested to appear in the ground-state band of ^{156}Dy are not supported by the transition probabilities determined in this work. Constant transition quadrupole moments were found in the g.s.b. ($Q_t \approx 6.5\ e\,$b), confirming the calculations made earlier within semimicroscopic mean-field approaches [8,11] which predict no change of the collectivity in the spin region up to $I = 14\hbar$. Thus, the $B(E2)$ transition strengths within the g.s.b. deviate significantly from the expectations of the X(5) critical point symmetry. In contrast, the intraband $B(E2)$ transition strengths in the first excited band follow the predicted X(5) pattern. Although their experimental uncertainties are relatively large, they may indicate a gradual transition away from X(5) changing the g.s.b. but keeping the X(5)-like first excited band. The interband transition strengths from the latter band point to a partial agreement with the X(5) model. An IBA fit helps to position ^{156}Dy in the transitional region between spherical and deformed nuclei. The results of the fit and empirical considerations reveal that in ^{156}Dy the γ degree of freedom (or the triaxiality) plays a more important role than in the recently established X(5) nuclei ^{152}Sm,^{150}Nd, and ^{154}Gd. A fit of the data using the general collective model points to a deeper collective potential $V(\beta, \gamma)$ in ^{156}Dy, which may be also a reason for the differences in the spectroscopic properties of ^{156}Dy and the neighboring $N = 90$ isotones exhibiting an X(5) character.

ACKNOWLEDGMENTS

One of us (P.P.) would like to thank his colleagues from the University of Cologne for their kind hospitality. This

work was supported by the BMBF (Germany) under Contract No. 06K-167, by the European Union TMR Programme under Contract No. HPRI-CT-1999-00083, and by the U.S. DOE under Grant No. DE-FG02-91ER-40609.

[1] H. R. Andrews, D. Ward, R. L. Graham, and J. S. Geiger, Nucl. Phys. **A219**, 141 (1974).
[2] R. M. Lieder, H. Beuscher, W. F. Davidson, A. Neskakis, C. Mayer-Böricke, Y. El Masri, P. Monseu, J. Steyart, and J. Vervier, Phys. Lett. **B49**, 161 (1974).
[3] C. W. Reich, Nucl. Data Sheets **99**, 753 (2003).
[4] D. Ward, H. R. Andrews, O. Häusser, Y. El Masri, M. M. Aléonard, I. Yang-Lee, R. M. Diamond, F. S. Stephens, and P. A. Butler, Nucl. Phys. **A332**, 433 (1979).
[5] H. Emling, E. Grosse, R. Kulessa, D. Schwalm, and H. J. Wollersheim, Nucl. Phys. **A419**, 187 (1984).
[6] H. Emling, I. Ahmad, P. J. Daly, B. K. Dichter, M. Drigert, U. Garg, Z. W. Grabowski, R. Holzmann, R. V. F. Janssens, T. L. Khoo, W. C. Ma, M. Piiparinen, M. A. Quader, I. Ragnarsson, and W. H. Trzaska, Phys. Lett. **B217**, 33 (1989).
[7] T. K. Alexander and J. S. Forster, Adv. Nucl. Phys. **10**, 197 (1978).
[8] M. L. Cescato, Y. Sun, and P. Ring, Nucl. Phys. **A533**, 455 (1991).
[9] Y. Sun and J. L. Egido, Nucl. Phys. **A580**, 1 (1994).
[10] V. Velazquez, J. G. Hirsch, Y. Sun, and M. W. Guidry, Nucl. Phys. **A653**, 355 (1999).
[11] K. H. Bhatt, S. Kahane, and S. Raman, Phys. Rev. C **61**, 034317 (2000).
[12] A. Dewald, S. Harissopulos, and P. von Brentano, Z. Phys. A **334**, 163 (1989).
[13] G. Böhm, A. Dewald, P. Petkov, and P. von Brentano, Nucl. Instrum. Methods Phys. Res. A **329**, 248 (1993).
[14] F. Iachello, Phys. Rev. Lett. **87**, 052502 (2001).
[15] R. F. Casten and N. V. Zamfir, Phys. Rev. Lett. **87**, 052503 (2001).
[16] R. Krücken, B. Albanna, C. Bialik, R. F. Casten, J. R. Cooper, A. Dewald, N. V. Zamfir, C. J. Barton, C. W. Beausang, M. A. Caprio, A. A. Hecht, T. Klug, J. R. Novak, N. Pietralla, and P. von Brentano, Phys. Rev. Lett. **88**, 232501 (2002).
[17] D. Tonev, A. Dewald, T. Klug, P. Petkov, J. Jolie, A. Fitzler, O. Möller, S. Heinze, P. von Brentano, and R. F. Casten, Phys. Rev. C **69**, 034334 (2004).
[18] A. Dewald, P. Sala, R. Wrzal, G. Böhm, D. Liebertz, G. Siems, R. Wirowski, K. O. Zell, A. Gelberg, P. von Brentano, P. Nolan, A. J. Kirwan, P. J. Bishop, R. Julin, A. Lampinen, and J. Hattula, Nucl. Phys. **A545**, 822 (1992).
[19] D. Bazzacco, in Procedings of the International Conference on Nuclear Structure at High Angular Momentum, Ottawa, 1992, Chalk River Report, AECL 10613, p. 386.
[20] P. Petkov, A. Dewald, O. Möller, B. Saha, A. Fitzler, K. Jessen, D. Tonev, T. Klug, S. Heinze, J. Jolie, P. von Brentano, D. Bazzacco, C. Ur, E. Farnea, M. Axiotis, S. Lunardi, C. Rossi-Alvarez, G. de Angelis, D. R. Napoli, N. Marginean, T. Martinez, M. Caprio, and R. F. Casten, Phys. Rev. C **68**, 034328 (2003).
[21] P. Petkov, Nucl. Instrum. Methods Phys. Res. A **349**, 289 (1994).
[22] P. Petkov, D. Tonev, J. Gableske, A. Dewald, and P. von Brentano, Nucl. Instrum. Methods Phys. Res. A **437**, 274 (1999).
[23] B. Saha, A. Dewald, O. Moller, R. Peusquens, K. Jessen, A. Fitzler, T. Klug, D. Tonev, P. von Brentano, J. Jolie, B. J. P. Gall, and P. Petkov, Phys. Rev. C **70**, 034313 (2004).
[24] L. C. Northcliffe and R. F. Schilling, Nucl. Data Tables A **7**, 233 (1970).
[25] J. F. Ziegler and W. K. Chu, At. Data Nucl. Data Tables **13**, 463 (1974).
[26] J. F. Ziegler and J. P. Biersack, in *Treatise on Heavy-Ion Science*, edited by D. A. Bromley (Plenum, NewYork, 1985), Vol. 6, p. 95.
[27] L. P. Ekstroem and A. Nordlund, Nucl. Instrum. Methods. A **313**, 421 (1992).
[28] K. S. Krane, R. M. Steffen, and R. M. Wheeler, Nucl. Data Tables **11**, 351 (1973).
[29] A. Bohr and B. R. Mottelson ,*Nuclear Structure* (Benjamin, New York, 1975), Vol. 2.
[30] A. Bohr and B. R. Mottelson, Dan. Mat. Fys. Medd. 30, no. 1 (1955).
[31] W. Nazarewicz, M. A. Riley, and J. D. Garett, Nucl. Phys. **A512**, 61 (1990).
[32] K. Heyde, P. Van Isacker, J. Jolie, J. Moreau, and M. Waroquier, Phys. Lett. **B132**, 15 (1983).
[33] K. Heyde, J. Jolie, P. Van Isacker, J. Moreau, and M. Waroquier, Phys. Rev. C **29**, 1428 (1984).
[34] D. S. Chuu and S. T. Hsieh, Phys. Rev. C **38**, 960 (1988).
[35] M. A. Caprio, N. V. Zamfir, R. F. Casten, C. J. Barton, C. W. Beausang, J. R. Cooper, A. A. Hecht, R. Krücken, H. Newman, J. R. Novak, N. Pietralla, A. Wolf, and K. E. Zyromski, Phys. Rev. C **66**, 054310 (2002).
[36] F. Iachello and A. Arima, *The Interacting Boson Model* (Cambridge University, Cambridge, 1987).
[37] K. Heyde, J. Jolie, R. Fossion, S. De Baerdemacker, and V. Hellemans, Phys. Rev. C **69**, 054304 (2004).
[38] M. A. Caprio, Phys. Rev. C **72**, 054323 (2005).
[39] G. Gneuss and W. Greiner, Nucl. Phys. **A171**, 449 (1971).
[40] D. Troltenier, J. A. Marhun, and P. O. Hess, in *Computational Nuclear Physics*, edited by K. Langanke, J. A. Marhun, and S. E. Koonin (Springer, Berlin, 1991), p. 105.
[41] S. G. Rohozinski, J. Dobaczewski, B. Nerlo-Pomorska, K. Pomorski, and J. Srebrny, Nucl. Phys. **A292**, 66 (1977).